Microfluidic Flow-By reactors minimize energy requirements of electrochemical water treatment without adding supporting electrolytes

Omar Alrehaili, Ana S Fajardo, Sergi Garcia-Segura, Paul Westerhoff

Microfluidic Flow-By Reactors Minimize Energy Requirements of Electrochemical Water Treatment Without Adding Supporting Electrolytes

Authors: Omar Alrehaili[a,*], Ana S. Fajardo[b,c,d], Sergi Garcia-Segura[b], Paul Westerhoff[b]

[a] Civil Engineering Department, College of Engineering, King Saud University, Riyadh, Saudi Arabia.

[b] Nanosystems Engineering Research Center for Nanotechnology-Enabled Water Treatment, School of Sustainable Engineering and the Built Environment, Arizona State University, Tempe, AZ, 85287-3005, USA

[c] Sorbonne Université, CNRS, Laboratoire Interfaces et Systèmes Electrochimiques (LISE), 4 place Jussieu, F-75005, Paris, France

[d] Polytechnic Institute of Coimbra, Applied Research Institute, Rua da Misericórdia, Lagar dos Cortiços – S. Martinho do Bispo, 3045-093 Coimbra, Portugal.

*Corresponding author (oalrehaili@ksu.edu.sa), P.O.Box 800, Riyadh 12372, Saudi Arabia

Abstract

While electrode material advances show how electrochemical processes can degrade wide range of environmental pollutants, less research exists on how to lower energy requirements for electrolysis through innovation in reactor geometry that control mass transfer. Microfluidic devices with high electrode surface area to solution volume ratios offer unique insights since they can minimize mass transfer limitations in electrochemical reactors and decrease the energy requirements. Shortening interelectrode distances hold promise to overcome charge transfer limitations, which otherwise requires electrolytes addition for low conductivity drinking waters. To examine the interconnected effects of electrode separation distances and solute concentrations on mass transport and energy efficiency, electrochemical treatment using a model water pollutant (nitrite ion) was evaluated in a flow-by microelectromechanical system (MEMS) reactor where the electrodes were ~ 40 μm apart in microfluidic reactors. The performance was compared to conventional completely-mixed batch reactors with interelectrode distance of 1 cm. The microfluidic reactors showed decrease of electrical energy per order (EE/O) in one order of magnitude with the ability to degrade contaminants with concentrations as low as 5 mg/L without increasing the energy consumption with the absence of supporting electrolytes. This paper presents a promising approach to study and ultimately develop cost-effective electrochemical technologies by optimizing electrode separation distances, instead of increasing salinity which is often required to achieve sufficient conductivity in water but is counter producing low-salt potable drinking water.

Keywords: Microfluidics; Electrochemical treatment; energy; mass transport; diffusion; water treatment

1 Introduction

Electrochemical water treatment processes are promising technologies for the advanced removal of targeted pollutants from drinking water resources and wastewater treatment plants effluents, including advanced oxidation and electrocatalytic reduction processes[1–4]. Heterogeneous hydroxyl radicals (•OH) are electrogenerated from water at the anode's surface during electrochemical oxidation (EO) for indirect electrochemical oxidation process[5]. In electrocatalytic reduction, electroactive species gain electrons through reduction reactions that occur at the cathode surface. In the case of nitrite reduction for example, the reduction mechanism can involve direct charge transfer process and indirect reduction from adsorbed hydrogen (H_{ads}) formed during the reduction of water. However, both electrochemically-driven reactions occur at the electrode surface making electrochemical treatments mass transfer limited processes. Limited mass transport might lead to high energy consumption when scaling-up electrified water treatment[6,7]. Different electrocatalysts can control selectivity of nitrite reduction towards nitrogen gas (N_2) or ammonium (NH_4^+)[8,9]. While preferential formation of N_2 is the most desired outcome when considering applications for drinking water, recent studies highly value NH_4^+ as an added value product when considering water reuse for agriculture[10,11].

The efficiency of an electrochemical reaction is controlled by charge or mass transfer[12,13]. Charge transfer is referred to the interfacial reaction at the electrode surface that is responsible of the redox reaction involving an electroactive species. When the reaction is governed by charge transfer, kinetics is determined by the number of electrons delivered and not by the target pollutant transport to the electrode surface. Charge transfer can be controlled by current intensity in the electrochemical process, higher current intensity leads to higher delivery of electrons per second which may accelerate the charge transfer rate. Hence, higher charge transfer can lead to a faster

abatement of target pollutant. However, increasing current intensity may decrease the total efficiency of the process determined by Faradaic efficiency (FE), the efficiency of charge (electron) transfer to a system facilitating an electrochemical reaction.

Mass transfer involves the transport of the target pollutant from/towards the electrode surface. This process is mainly governed by diffusion and migration of chemicals from the bulk solution to the electrodes surfaces where the electrochemical reactions occur[14,15]. Mass transfer by diffusion is controlled by diffusivity of individual species and thickness of diffusion layer that is influenced by the Reynold's number and solute concentration gradients between bulk solution and electrode surface[16,17]. Mass transfer by migration is driven by electrical potential gradients in the cell. High resistance in an electrochemical cell hinders mass transport where energy consumption increases for solutions with low conductivity due to ohmic drop. Solution conductivity has a direct impact on electrocatalytic activity[18]. The addition of supporting electrolyte decreases the resistance and diminishes the overall energy consumption[19–22]. However, adding salt could be expensive and may require additional removal of added chemicals. Furthermore, most research add > 50 mM of ionic strength (> 3000 μS/cm) to achieve sufficient background electrolyte concentrations. The secondary drinking water standard in the United States of America for total dissolved solids (TDS) is 500 mg/L (~ 750 μS/cm or ~12 mM). Therefore, most electrochemical studies have utilized conductivity levels far in excess of salt concentrations recommended for drinking water for aesthetic or health reasons.

Advances in micro and nanofluidics can tackle the issues of high energy consumption in water treatment processes[23]. Microfluidic reactors with micro inter-electrode distance could overcome electrochemical limitations of mass transfer and decrease energy consumption even with the absence of supporting electrolytes at low cell voltage[21,24–28]. The small distance between the

two electrodes accelerates and intensify the kinetic of mass transfer rate inside the reactor leading to the ability of achieving a continuous flow mode where pollutants are converted in a single passage of solution[29,30]. The ability to achieve a continuous flow reaction with short residence time allows flexibility on changing applied conditions as compared to a batch reactor. Most microfluidic reactors reported on the literature are based on building a commercially available filter press cell (flow-by-cell) made of polytetrafluoroethylene PTFE spacer (100-500 μm) to separate the two electrodes[7,29,30]. Other devices were made by micro-milled adhesive spacer for microchannel between two electrodes[21,30].

In this work, microfluidic devices were fabricated as a cross flow system between two electrodes based on microelectromechanical system (MEMS) fabrication techniques, where the interelectrode distance was 40 μm. The objective is to evaluate the impact of engineering reactor design on the electrochemical systems performance. As a model reaction, nitrite conversion was studied in electrochemical microfluidic reactors in a single pass as compared to bulk batch reactors without or with supporting electrolytes (variable salinity concentrations) and benchmarked using engineering figures of merit. Nitrite is regulated by the United States of America Environmental Protection Agency (EPA) with a maximum contaminant level (MCL) of 1 mg NO_2^--N/L. The influence of main parameters in electrochemical reactors such as current intensity and solution conductivity are considered. Electrical energy per order and electrical consumption were reported and compared for the electrical requirements between the two types of reactors.

2 Material and Method

2.1 Electrodes Preparation and Microfluidic Device Fabrication

All electrodes used in this work were made of platinum (Pt) and prepared in the lab using silicon (Si) wafers as substrates for all devices. Due to its high corrosion resistance and ability to prevent poisoning by reduction by-products, platinum electrodes prove to be excellent electrocatalysts for nitrate/nitrite reduction[2,31,32]. Platinum has been reported to have high selectivity for nitrate/nitrite reduction towards ammonium[33]. A Platinum layer of 100 nm were coated on wafers using thermal evaporation techniques. Preparing electrodes by thermal evaporation technique results in a homogeneous and smooth electrodes surface to avoid friction forces that might increase in microchannel as reported in other works[7].

Electrochemical microfluidic devices were fabricated based on microelectromechanical system (MEMS) techniques where the interelectrode distance (the distance between electrodes) is less than 50 μm (~40 μm) (Figure 1). Briefly, the platinum coated electrodes were further coated with epoxy polymer (SU-8) by a spin coater acting as a separation layer between the two electrodes in the device. The thickness of the epoxy layer determines the distance between the two electrodes in the microfluidic device and it is controlled by the viscosity of the polymer and the spin coat speed. The final result shows a thickness layer of ~40 μm. A channel was etched on the epoxy layer all the way to Pt surface on the wafer where solution pass though between the electrodes. Lastly, in order to connect the microchannel to macro reservoirs, a microfluidic delivery device fabrication (stamp) is needed. The delivery device was made of polydimethylsiloxane (PDMS) and connected to a syringe pump through needles and luer connector (silicon tubes). More details in the device fabrication were reported in the supporting information (Figure S1).

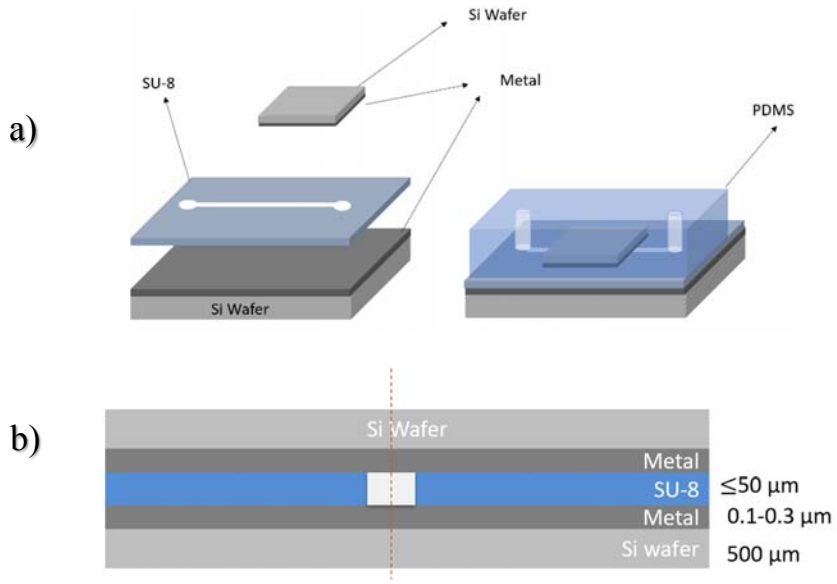

Figure 1: Schematic of the microfluidic device fabricated by soft lithography. a) 3-D of the device components. b) a cross view of the device.

2.2 Operation of Electrochemical Reactors

Experiments were conducted with solutions of 50 mg-N/L of nitrite (equivalent to 3.56 mM of potassium nitrite (KNO_2) and 165 mg/L as nitrite) with initial pH 6.5. Conductivity was modified by adding Na_2SO_4 as supporting electrolyte with concentrations ranging from 0 up to 100 mM of Na_2SO_4. Nitrite was used to evaluate the reactors performance as its decay reaction by platinum electrodes is well achieved. The applied current intensity was varied from 1 mA to 160 mA using a power supply (Tenma DC 72-2720). These solutions were treated galvanostatically using the microfluidic electrochemical reactor and a batch reactor illustrated in Figure 2, which operation is described below.

Microscale microfluidic devices. Experiments were conducted in continuous flow reactors where electrochemical reactions occur in a single pass through one channel of 500 µm wide, 40 µm interelectrode distance and 25 mm length. Solution is delivered to the microreactor by a syringe pump with flowrate ranges between 0.02 mL/min and 0.65 mL/min. The corresponding residence

time to the applied flowrate determines hydraulic residence time (HRT) for the electrochemical reaction in the reactor. Samples were collected at the outlet.

Macroscale batch reactors. Experiments were conducted with 100 mL solutions in a beaker under magnetic stirring at 700 rpm to ensure target pollutant transport from/towards the electrode surface in the reactor. The reactor is equipped with two 4.5 cm^2 platinum (Pt) electrodes, prepared under same conditions than the electrodes used in microfluidic set ups. The interelectrode distance was kept at 1 cm for all experiments.

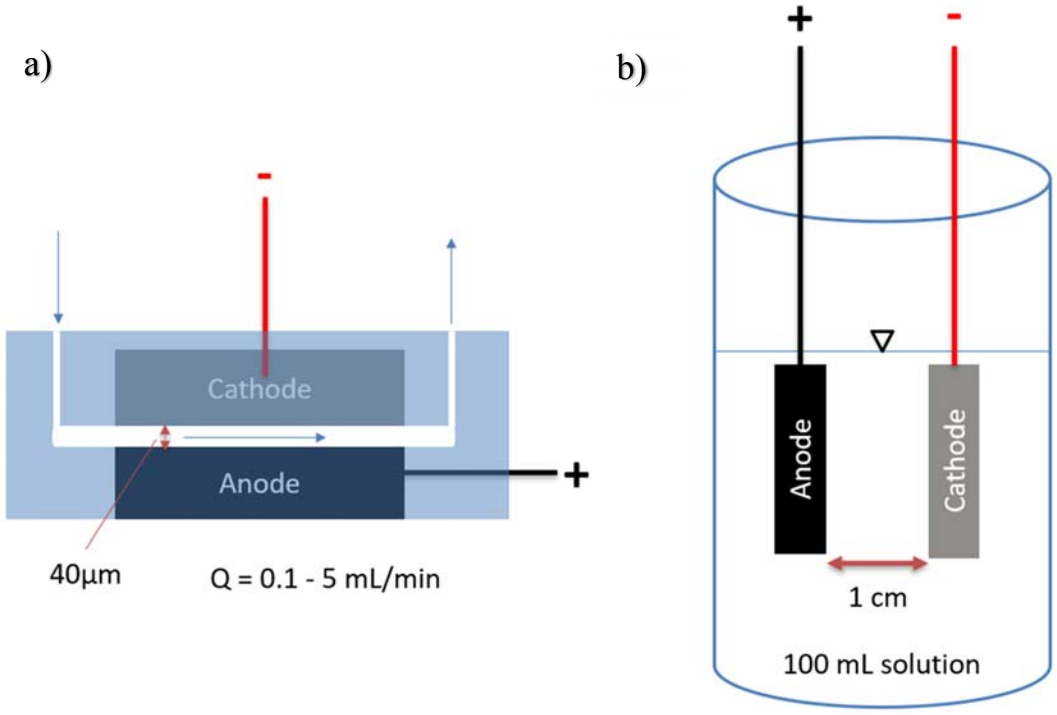

Figure 2: Schematics of **a)** a flow-by microfluidic reactor where interelectrode distance is 40 µm and **b)** a batch reactor in a beaker where interelectrode distance is 1 cm.

2.4 Measurements and Analysis

Conductivity of the solutions was measured by Thermo Scientific conductivity meter (Orion Star A322 Portable) and the pH measurements were conducted by Thermo Scientific pH-meter (Orion Star A221). Samples were withdrawn from reactors at a given time and were analyzed for conversion of nitrite by UV Spectrophotometery (Hach DR6000) at the maximum absorption

wavelength of nitrite of λ_{max} = 354 nm and Ion Chromatography (Metrohm 930 Compact IC Flex). The corresponding potential was taken continuously for any new run or at any change in experimental parameters. Microchannel dimensions were measured by Bruker XT Profilometer.

The effectiveness of the electrochemical reduction was evaluated in terms of Faradaic efficiency (FE), which counts for the number of electrons consumed in the electrochemical process relative to the theoretically expected conversion governed by Faraday's law and determined by Eqs. (1) and (2)[2,34]:

$$FE = \frac{Q_{exp}}{Q_{thoer}} \times 100 = \frac{n \times F \times N_{i-r} \times Q_r}{3600 \times I} \times 100 \quad \text{(Flow-by reactor)} \tag{1}$$

$$FE = \frac{Q_{exp}}{Q_{thoer}} \times 100 = \frac{n \times F \times N_i}{3600 \times I \times t} \times 100 \quad \text{(Batch reactor)} \tag{2}$$

where Q_{exp} is the experimental charge consumed in the reaction in Coulomb (C), Q_{theor} is the total charge circulated in (C), n is the amount of electrons required per mol of product (mol), F is the Faraday constant (96,487 C mol^{-1}), $N_{i\text{-}r}$ is the amount of product generated per volume (mole/L), Q_r is the flowrate in the microfluidic reactor (L/h), N_i is the amount (mol) of product generated during the electrolysis, I is the applied current in amperes (A), t is the reaction time in hours (h), and 3600 is a unit conversion factor (3600 s/h).

To compare batch and microfluidic reactors, the electrical energy requirements were benchmarked using engineering figures of merit. The electrical energy per order (EE/O) (kWh m^{-3} $order^{-1}$) is defined as the electric energy required to remove a contaminant by one order of magnitude in a unit volume, as estimated by Eqs. (3) and (4)[2,35]:

$$EE/O = \frac{E_{cell}\, I}{Q\, Log\, (\frac{C_0}{C})} \quad \text{(Flow-by reactor)} \tag{3}$$

$$EE/O = \frac{E_{cell}\, I\, t}{V_s\, Log\, (\frac{C_0}{C})} \qquad \text{(Batch reactor)} \tag{4}$$

where E_{cell} is the average cell potential in volt (V_s), Vs is the solution volume treated in liter (m^3), Q is flowrate for the continuous flow system in cubic meter per hour (m^3/h), and C and C_0 are the final and initial concentration of pollutant (mg/L). The electrical energy consumption EC (kWh g^{-1}) required for the degradation of a unit mass of contaminants was estimated by Eqs. (5) and (6)[35,36]:

$$EC = \frac{E_{cell}\, I}{Q\, (C_0 - C)} \qquad \text{(Flow-by reactor)} \tag{5}$$

$$EC = \frac{E_{cell}\, I\, t}{V_s\, (C_0 - C)} \qquad \text{(Batch reactor)} \tag{6}$$

Two methods are used to compare reactors performance in terms of mas transfer coefficient: (i) experimentally based on limiting current measurements using linear sweep voltammetry[14,15,37], and (ii) empirically by using dimensional analysis[15,38]. In this research, dimensional analysis is considered as commonly used method to determine mass transfer coefficient rate based on the three nondimensional groups: the Sherwood number (Sh) described by Eq. (7)[15]; the Reynolds number (Re) defined according to Eqs. (8) and (9)[39]; and the Schmidt number (Sc) following Eq. (10). These groups are related to the mass transfer coefficient k_m (m/s) which was calculated from Eq. (11)[15] for Re # < 2000:

$$Sh = 3.33\, Re^{1/3} Sc^{1/3} Le^{1/3} \tag{7}$$

$$Re = \frac{u d_h}{\nu} \qquad \text{(Flow-by reactor)} \tag{8}$$

$$Re\ \frac{D_r^2\, n \rho}{\mu} \qquad \text{(Batch reactor)} \tag{9}$$

$$Sc = \frac{\nu}{D} \tag{10}$$

$$k_m = \frac{Sh\ D}{d_h} \quad (11)$$

where d_h is the equivalent diameter of the channel (m), D is the diffusivity of nitrite in water (m^2/s), Le is the ratio of d_h over electrode length, u is the velocity of fluid (m/s), $\boldsymbol{\nu}$ is the kinematic viscosity of the fluid (m^2/s), D_r is impeller diameter (m), n is rotation speed (rotation/s), ρ is the density of solution kg/m^3), and μ is the viscosity if fluid (P.s) . Also, the diffusion layer thickness δ (m) affects mass transfer in electrochemical cell as a function of ion diffusivity and diffusion transfer coefficient. Since most of mass transfer occurs due to diffusion[34], mass transfer coefficient assumed to be due diffusion where diffusion layer thickness was calculated by Eq. (12)[37,40]:

$$\delta = \frac{D}{k_m} \quad (12)$$

3 Result and Discussion

Electrolysis were performed in microfluidic and conventional batch reactors with interelectrode distance of 40 μm and 1 cm, respectively. The electrolysis performance metrics were obtained for nitrite decay, EE/O, and EC by varying current density and solution conductivity with and without adding supporting electrolytes.

3.1 Electrolysis Performance for Nitrite Conversion

Electrolysis were conducted to evaluate the two reactors for nitrite decay over time without adding supporting electrolytes. The applied current density was fixed at j= 18 mA/cm^2, with corresponding current intensity of I ~3 mA for microfluidic reactor and I = 80 mA for batch reactor. Figure 3 shows nitrite decay in microfluidic reactor that occurs in single pass where the flowrate through the reactor channel determines the hydraulic residence time (HRT). Slower

232 flowrates lead to longer HRT and therefore improved the percentage of nitrite reduction achieved
233 per single pass, resulting in larger amounts of charge transferred to the solution with increase HTR.
234 The flowrate was varied from 0.021 to 0.5 mL/min with a HRT corresponding to 1.43 to 0.06
235 second (s). Triplicate measurements of nitrite abatement were conducted at each HRT experiments
236 and the results were very consistent for the microfluidic reactors at average standard deviation (SD
237 = ± 3 x 10^{-3} mg/L).

238 To compare the performance of both reactors for nitrite decay, Figure 3 also shows the
239 decay of nitrite over time in a 100 mL solution in a batch reactor. Nitrite decay improves by
240 increasing reaction time where ~95% nitrite reduction was achieved after 3 hours runs. The decay
241 rate in microfluidic reactor was faster than batch reactor, where 95% reduction was achieved in
242 ~1.5 s as compared to 3 hours in batch reactor at fixed current density. Faradic efficiency (FE) was
243 calculated to measure the efficiency of the reactors by Eq. (1) and (2) for the conversion of nitrite
244 and the production of ammonium as expected from the reduction of nitrite by Pt cathode (Figure
245 3). For both reactors, FE decreased by increasing the reaction time. Even with short reaction time
246 in microfluidic reactors, FE for the two reactors were significantly different (by *t*-test) at more than
247 two times higher in microfluidic reactor at an average of ~ 9% as compared to batch reactor
248 (~3.5%) due the high area of electrode to solution volume ratio (~ 250 cm^2/mL) as compared to (~
249 0.045 cm^2/mL) in batch reactor. FE for converting nitrite to ammonium is consistent with literature
250 reports ranging from 2% to 9 %[41,42].

251

252

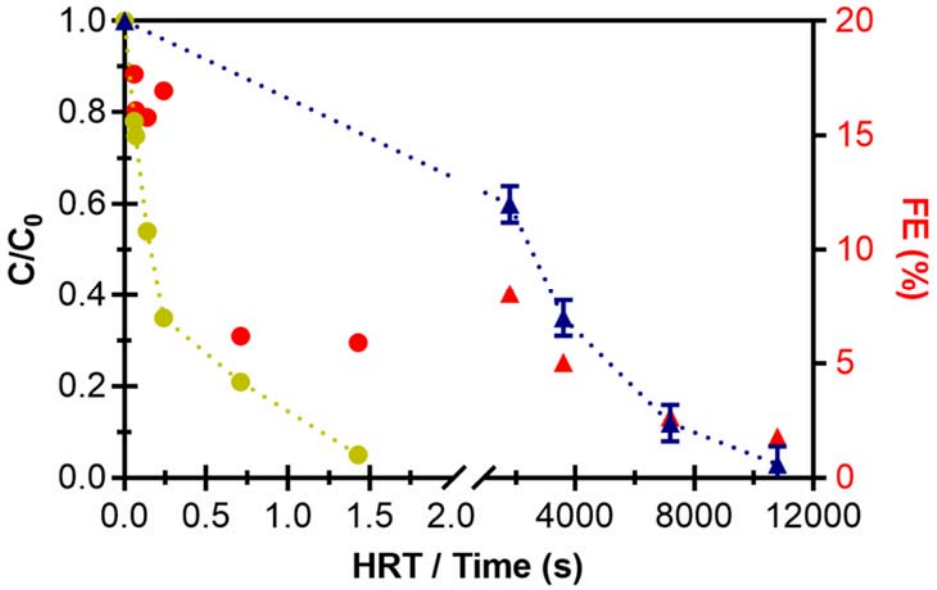

Figure 3: Nitrite decay over time by Pt cathode and Faradaic efficiency (red) in batch reactors ( ) and microfluidic reactors ( ). Current density is fixed at j = 18 mA/cm^2, initial concentration C_0 = 50 mg-N/L and conductivity was 0.53 mS/cm^2 and pH = 6.5. Error bars represent standard deviation for triplicate measurements (< 1% standard deviation in percentage nitrate reduction based upon triplicate experiments for microfluidic reactor).

3.2 Kinetics Reaction Rate Constant

The electrolysis rate in the conventional batch reactor follows pseudo first-order kinetics for nitrite decay ($r_{NO2^-} = -k\,[NO_2^-]$) with an apparent reaction rate constant of k = 3 x 10^{-3} s^{-1} (Figure 4a). On the other hand, rates in the microfluidic reactor exhibit a two-stage kinetic as a function of HRT. Figure 4b shows nitrite rates in the microfluidic reactor first follow zero-order kinetics ($r_{NO2^-} = -k'$) with faster decay rates of nitrite at shorter HRT (0.06 – 0.14 s) followed by pseudo first-order kinetics at longer HRTs (0.24 to 1.42 s). First, the faster kinetic rate occurs until reaching a limiting current density (the maximum current to achieve a desired reaction before to the simultaneous discharge of extraneous ions), when it then becomes mass transfer limited by diffusion as described previously in kinetic models. The zero-order kinetics ($r_{NO2^-} = -k'$) have k'

= 4.4 mol L^{-1} s^{-1} at lower HRTs while first-order kinetics for nitrite decay ($r_{NO2-} = - k [NO2-]$) have $k = 1.1$ s^{-1} at higher HRTs.

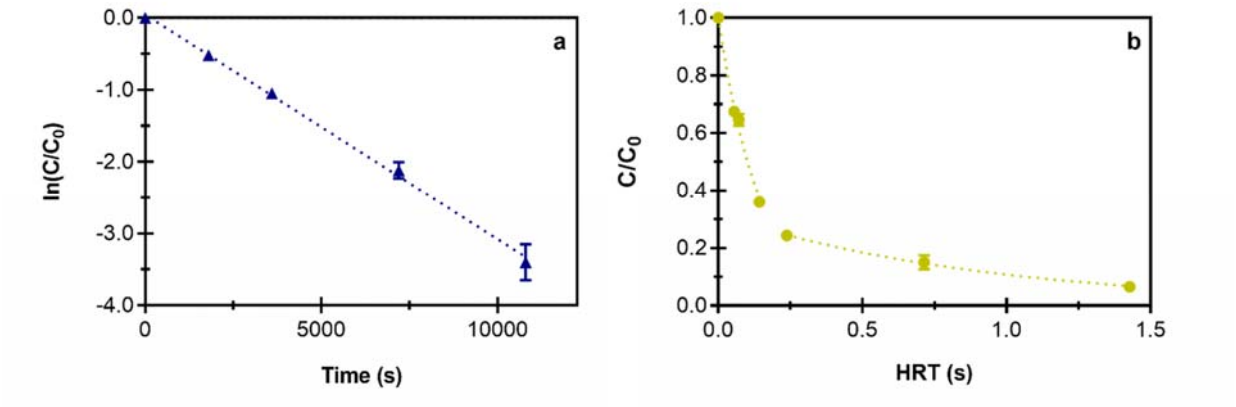

Figure 4: Nitrite decay data for a) batch reactors (▲) as it fits first order kinetics and b) microfluidic reactor (●) as showing two trends, zero and first order kinetics. Initial concentration of nitrite $C_0 = 50$ mg-N/L, conductivity of 0.53 mS/cm and pH = 6.5. Error bars represent standard deviation for triplicate measurements (SD = $3x10^{-3}$ mg/L of nitrite decay for microfluidic reactors).

3.3 The Effect of Current Density on Microfluidic Electrolysis Performance

The applied current density (j) is an important parameter for electrochemical processes since j controls the reaction kinetics. At high applied current, more electrons are delivered per second leading to enhanced transfer of electrons between the electrodes and the electroactive species in solution. Higher availability of electrons may lead to an increase in reaction rates. However, applied currents above the current limit result in a transition towards mass transfer limitation, where the degradation rate becomes limited by diffusion of electroactive species (*i.e.*, nitrite) towards the electrode surface. Then, the additional electrons transferred are used in parasitic reactions such as hydrogen evolution reaction from water reduction. When increasing current has no or minimum effect on electrolysis performance, the reactor is considered a mass transfer limited.

To evaluate the effect of current density on nitrite removal in the microfluidic reactor, Figure 5 shows the electrolysis performance for nitrite reduction at different applied current density j ranging from 18 mA/cm^2 (I = 3 mA) up to 640 mA/cm^2 (I = 80 mA). The initial concentration of nitrite was 50 mg-N/L (0.53 mS/cm) and no supporting electrolytes were added. Increasing the HRT in the cell improves the reduction percentage attained for both applied currents. However, at j = 640 mA/cm^2, nitrite reduction increased by an average of 20% as compared with reactors where j = 18 mA/cm^2 was applied due to the increase of the amount of charge passed through the electrodes. However, increasing the current also leads to the increase of the energy consumption in the reactor.

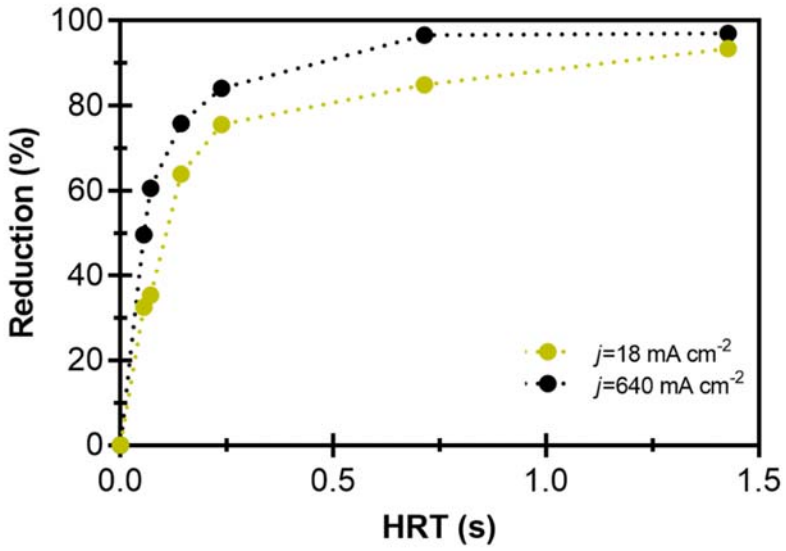

Figure 5: The effect of applied current density on nitrite reduction over time in microfluidic reactors. Interelectrode distance = 40 μm, initial concentration of nitrite is 50 mg-N/L (0.53 mS/cm) and pH = 6.5. No supporting electrolytes were added. Error bars represent standard deviation for triplicate measurements (SD < 1% in percentage of nitrite reduction based upon triplicate experiments).

3.4 The Effect of Current Density on Energy Requirements

The effect of current density on electrical energy requirements is evaluated by testing a range of currents at a fixed reaction time. Figure 6 shows the increase in electrical energy per order (EE/O) (kWh m^{-3} $order^{-1}$) of the nitrite reduction calculated by Eq. (3) and (4) for both microfluidic and batch reactors at applied current density ranges from j= 8 mA/cm^2 to 40 mA/cm^2. In the microfluidic reactor, the experiment proceeds at fixed HRT of 0.24 s, whereas reaction times up to 1 hour were monitored in the conventional batch reactor. Supporting electrolytes were not added for both reactors.

In the microfluidic reactor (Figure 6), nitrite reduction of 66% was achieved at low current density of j= 8 mA/cm^2 (I = 1 mA) at the given HRT. Nitrite reduction then increased by 13% when the current density was raised to j = 40 mA/cm^2 (I = 5 mA). The EE/O in the microfluidic reactor increased four-fold when the current density increases by factor of five. On the other hand, nitrite reduction in batch reactor was at ~ 50% at lower current density j= 8 mA/cm^2 (I = 40 mA) and increased by 19% when current density increased to j= 40 mA/cm^2 (I = 160 mA). The electrical energy per order increased by nine-fold when the current density was increased by a factor of five (Figure 6). However, the microfluidic reactor achieved the same nitrite reduction and more when compared to the batch reactor with at least one order of magnitude lower electrical energy required when current density was j > 20 mA/cm^2. This is due the increase in mass transfer rate achieved by small micrometric distance between the two-electrode that leads to low resistance in the reactor.

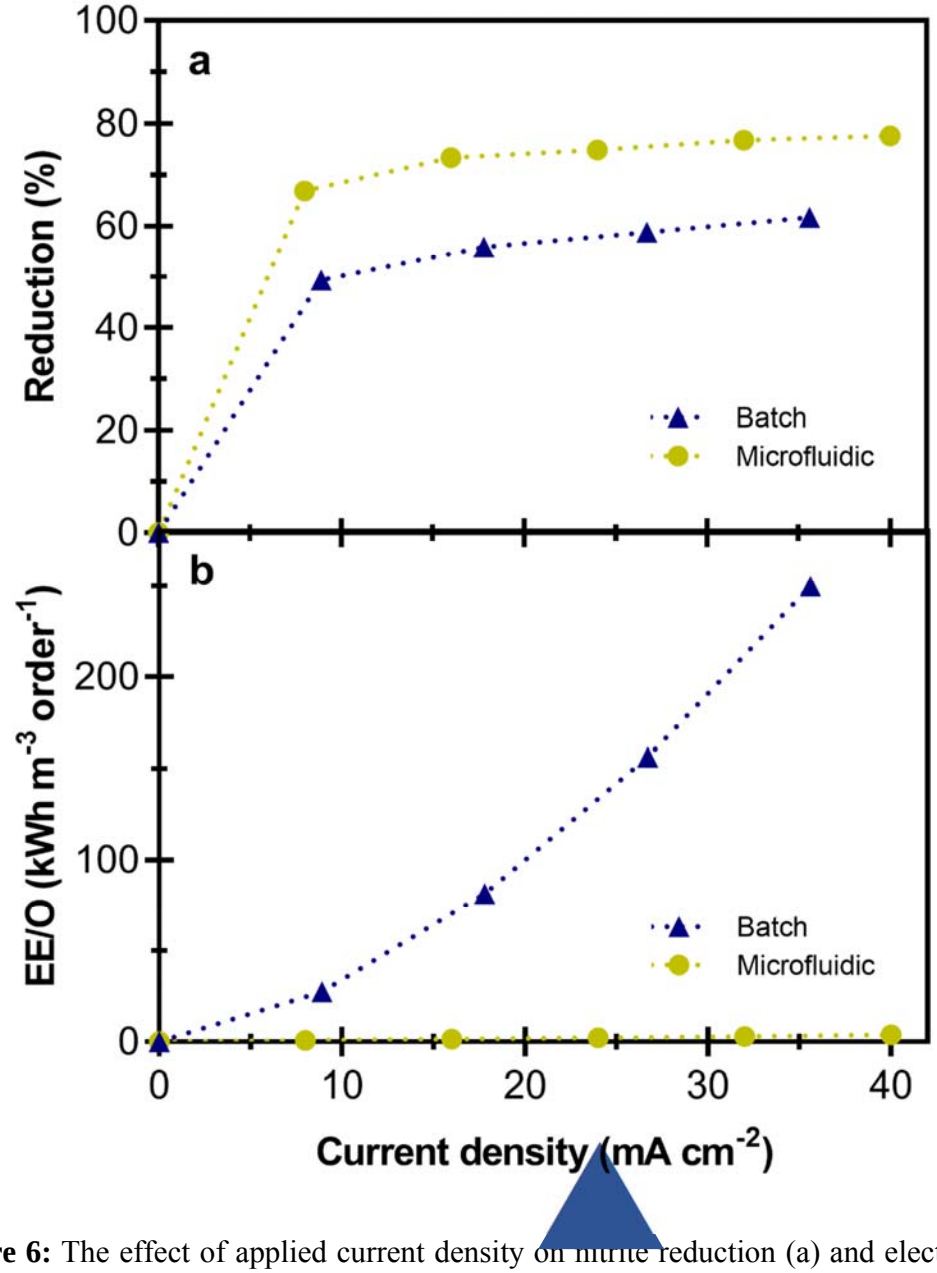

Figure 6: The effect of applied current density on nitrite reduction (a) and electrical energy per order requirement (b) for the batch reactor ( ) and for the microfluidic reactor ( ). Initial concentration of nitrite is 50 mg-N/L (0.53 mS/cm and pH = 6.5). The flowrate of the microreactor is fixed at Q = 0.125 mL/min (HRT = 0.24 s). For batch reactor, the reaction time is fixed at one hour for 100 mL solution. No supporting electrolytes were added. Error bars represent standard deviation for triplicate measurements.

5.3.5 The Effects of Electrolyte Concentrations on Energy Requirements

The conductivity of an aqueous solution indicates the ability of the solution to conduct electric current. By increasing the concentration of ions in solution, conductivity will be increased and hence resistance in the solution is decreased between the electrodes. Thus, the addition of supporting electrolytes (non-electroactive ions) is used to increase the solution conductivity, decrease the diffusion layer on the electrode, and decrease the cell potential. Enhancing the solution conductivity, it also decreases the resistance in the medium and diminishes the overall energy consumption. Moreover, adding supporting electrolytes to the system may affect the mass transfer in the electrochemical reactors by eliminating the mass transfer by migration leading to dominant mass transfer by diffusion. However, presence in high concentrations of other electrolytes could interfere with the electrochemical reactions of interest by enacting competitive reactions. Also, the requirement of salt addition may increase the operation costs and might require additional removal of salt content after treatment.

Figure 7 shows nitrite reduction and electrical energy requirements in batch and microfluidic reactors for different initial nitrite concentrations with and without adding supporting electrolytes. The conventional batch reactor experiments were conducted by using nitrite solutions (5 – 50 mg-N/L) at fixed current density (j = 18 mA/cm^2) and fixed reaction time of one hour of 100 mL solutions (Figure 7a). At first, electrolysis runs for solutions with nitrite concentration < 50 mg-N/L (< 1 mS/cm) without the addition of supporting electrolytes were not achieved due to the high potential in the cell (> 61 V). For other nitrite solutions, there is no significant effect on the reduction by increasing solutions conductivity as indicted in Figure 3. However, the EE/O was at highest for solutions with lower conductivity and was reduced by 80% when 50 mM Na_2SO_4 was added as supporting electrolyte.

364 The small interelectrode distance in microfluidic reactors is an alternative approach to
365 enable and enhance the electrolysis without adding supporting electrolytes. Microfluidic reactors
366 can also perform high nitrite reductions at low concentration without increasing energy
367 requirements. As a comparison to the batch reactor, Figure 7b shows nitrite reduction and electrical
368 energy requirement in microfluidic reactors using same nitrite solution (5 – 50 mg-N/L) with and
369 without adding supporting electrolytes at fixed current density (18 mA/cm^3) and HRT (0.24 s).
370 When the conductivity of the solution increased by 3 order of magnitude, the electrical energy per
371 order increased only by 25%. Nitrite reduction was the same or higher for the solution with low
372 conductivity. At low nitrite concentration (5 mg-N/L, 0.06 mS/cm), the microfluidic reactor
373 achieved ~91% reduction leading to a final concentration less than the maximum contaminant
374 level of nitrite as regulated by the US Environmental Protection Agency (EPA, MCL = 1 mg-
375 N/L).[18].
376 Electrical energy per order requirements in the microfluidic reactors (2.2 kWh m^{-3} $order^{-1}$)
377 represent only 5% of the energy required in the batch reactor (64 kWh m^{-3} $order^{-1}$) to treat 50 mg-
378 N/L nitrite without adding supporting electrolytes and more than 4 times lower even when
379 supporting electrolytes were added (13 kWh m^{-3} $order^{-1}$ with 50 mM Na_2SO_4) in the batch reactor.
380 Electrical energy per order usually ranges from 20 - 60 kWh m^{-3} $order^{-1}$ for nitrite reduction as
381 previously reported[33]. Note that these results evidence the promissory performance of microfluidic
382 devices but do not analyze the effect of other co-existing species. For instance, recent experimental
383 research demonstrates that the presence of water hardness ionic species (i.e., Ca^{2+}, Mg^{2+}) may
384 induce the precipitation of inorganic scaling on the surface of the cathode[43]. Precipitation is
385 favored by the high alkaline pH localized on the cathode surface. The formation of inorganic
386 scaling on the cathode inhibits transport of electroactive species from/towards the electrocatalytic

sites of the electrode surface and therefore decreases performance of electrochemical reduction of nitrite. Effects and challenges that may arise from the treatment of real water matrices are beyond the scope of this study, but should not be overlooked when considering technology translation.

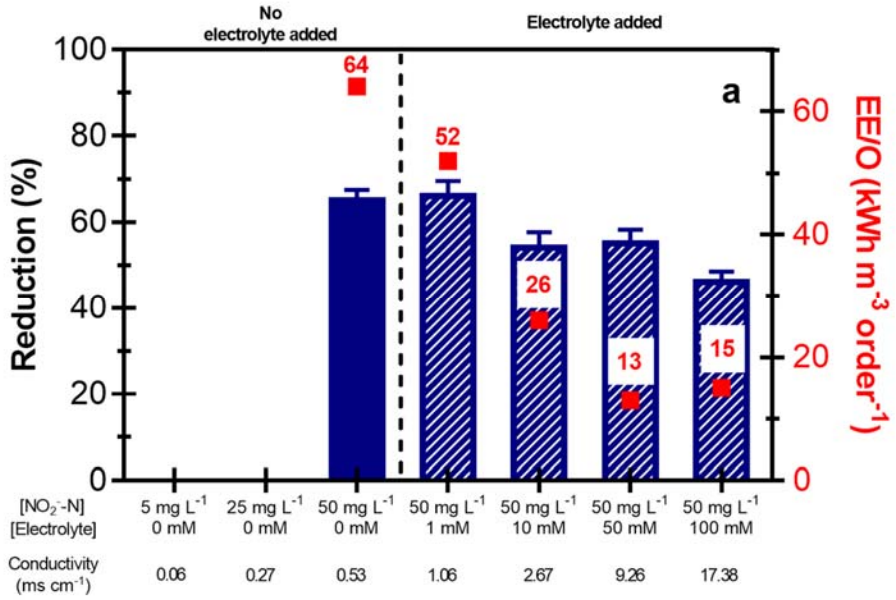

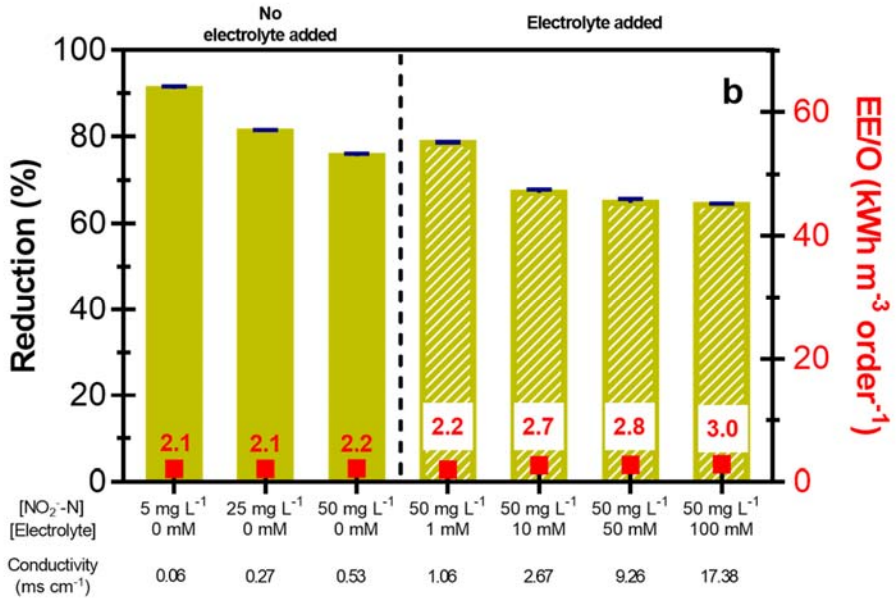

Figure 7: The effect of conductivity and the addition of supporting electrolytes at fixed current density (j= 18 mA/cm^2) on nitrite reduction (bars) and electrical energy per order (■) for the **a)** batch reactor and the b) microfluidic reactor. Initial concentration of nitrite is varied to 5, 25, and

50 mg-N/L at pH = 6.5. Supporting electrolytes were added to 1, 10, 50, and 100 mM of Na_2SO_4 for 50 mg-N/L N solutions where corresponding initial conductivity was reported. The flowrate of microfluidic reactor is fixed at Q = 0.125 mL/min (HRT = 0.24 s). Batch reactor was run at one-hour reaction time for 100 mL solutions. Error bars represent standard deviation for triplicate measurements.

3.6 Energy Consumption in Micro and Conventional reactors

To compare the two reactors in terms of energy consumption required to remove a unit mass of contaminants, nitrite electrolysis was performed for an energy consumption level as calculated using Eq. (5) and (6). Figure 8 shows the energy consumption for the removal of nitrite to achieve at least 90% reduction in batch and microfluidic reactors under the same conditions with and without the addition of supporting electrolytes. The initial concentration was 50 mg-N/L N and current density was fixed at 18 mA/cm^2. Adding supporting electrolytes had no effect on the energy required in microfluidic reactor for a reduction of nitrite > 90%. The microfluidic reactor consumed one order of magnitude of energy lower than batch reactor with the absence of supporting electrolytes. Even with the addition supporting electrolytes, the microfluidic reactor consumed half the energy required as compared to batch reactors.

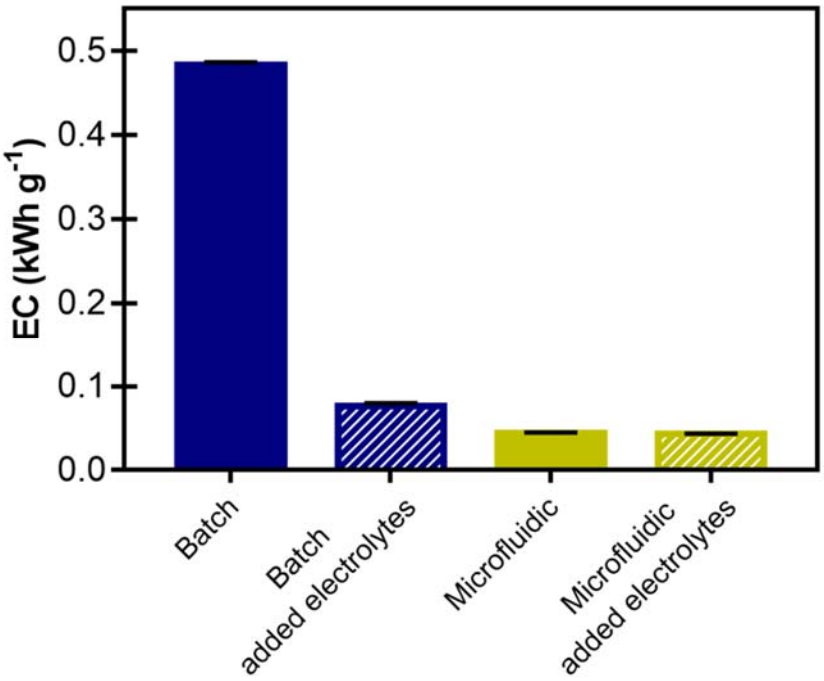

Figure 8: Electrical energy consumption required after 90% removal of nitrite in batch and microfluidic reactors at fixed current density (j= 18 mA/cm^2). Initial concentration of nitrite is C_0 = 50 mg-N/L and 50 mM Na_2SO_4 added as supporting electrolyte. The flowrate of microfluidic reactor to achieve > 90% removal was at Q = 0.02 mL/min (HRT = 1.43 s) and the batch reactor was run for three hours for 100 mL solutions. Error bars represent standard deviation for triplicate measurements.

3.7 Mass Transfer and Diffusion Layer Thickness

Superior mass transfer for nitrite in microfluidic reactors was achieved with lower energy as compared to batch reactor. The EE/O is a figure of merit to measure energy input and reaction. In microfluidic reactors even with increase in current we still maintain a low cell potential (< 5 V) where kinetics is fast (k = 1-7 s^{-1}). The enhanced mass transfer in microfluidic reactors can be reported by higher mass transfer coefficient (k_m) and the compressed diffusion layer (δ) as compared to batch reactor (Table 1). Mass transfer coefficients for microfluidic and batch reactors were calculated from equations (7-11). In microfluidic reactors, k_m increased with increasing flowrate where the Reynolds number (*Re#*) is increased. The diffusion layer thickness on the other

hand decreased with increasing flowrate Eq. (12). As compared to batch reactor, k_m in microfluidic reactor is reported to be two orders of magnitude higher than batch reactor which is consistent with the previously reported values of k_m for micro channel with much higher electrode area[4]. For the batch reactor, k_m was estimated to be 5.9×10^{-4} cm/s and was constant with previously reported values[44]. The diffusion layer was estimated based on k_m to be at least one order of magnitude lower in microfluidic reactors (5-17 μm) as compared to batch reactor (290 μm). Therefore, the compressed diffusion layer in microfluidic reactors led to a higher mass transfer due to the lower resistance where lower electrical energy is required.

Table 1: Non-dimensional groups, mass transfer coefficient and diffusion layer thickness for different flowrate in microfluidic and batch reactor.

Flowrate Q (mL/min)	***Re #***	***Sc #***	***Sh #***	***Le***	***km (cm/s)***	***δ (μm)***
Microfluidic Reactor						
0.02	1.30	588	4.32	3×10^{-3}	0.010	17.2
0.04	2.59		5.43		0.012	13.6
0.13	7.72		7.78		0.018	9.5
0.21	12.96		9.23		0.021	8.0
0.42	25.93		11.61		0.027	6.4
0.50	30.86		12.29		0.028	6.0
0.63	38.89		13.27		0.030	5.6
Batch Reactor						
700 rpm (stirring)	2037	588	73.21	0.01	5.9×10^{-4}	290

4 Summary and Conclusions

The small distance between the two electrodes in electrochemical microfluidic reactors shows promises to overcome mass transfer limitation associated with the high energy requirements in conventional electrochemical technologies. Electrolysis was performed for nitrite reduction in a microfluidic reactor (interelectrode distance = 40 μm) and a conventional batch reactor (1 cm interelectrode distance) by the variations of three parameters: 1) current density, 2) initial concentration of contaminants, and 3) the addition of supporting electrolytes. Unlike conventional batch reactors, it was found that the performance of the microfluidic reactor with electrode separations of < 100 μm is less dependent on the addition of salt concentrations above levels suitable for drinking water. Note that addition of salt to increase conductivity is not as critical for microfluidic systems than for conventional reactors where electrodes are spaced millimeters or greater distances apart. The main conclusions from this research are:

- Microfluidic reactors achieved > 95% reduction of nitrite in less than 1.5 seconds where the batch reactor required 3 hours for the same decay percentage. The reaction rate constant was 3 orders of magnitude faster with the microfluidic rector than with the batch reactor.
- Even with short time of reaction in the microfluidic reactor, the efficiency was more than two times higher at 95% reduction of nitrite as compared to batch reactors (measured by Faradaic efficiency).
- At low concentration of contaminants (5 mg/L nitrite) and low solution conductivity (0.06 mS/cm), the microfluidic reactor shows > 90% reduction of nitrite with no effect on energy requirements, whereas electrolytes were not successfully performed in conventional batch reactor due to high electrical potential (> 61 V).
- Electrical energy required to degrade nitrite by one order (EE/O) in the microfluidic reactor was one order of magnitude lower than the batch reactor without adding supporting electrolytes. Even when 50 mM of Na_2SO_4 was added as supporting electrolyte to the solution, EE/O was 4 time higher in batch reactors.
- Microfluidic reactors achieved > 90% reduction of contaminants by an order of magnitude lower energy consumption (EC) as compared to batch reactor without the addition of supporting electrolytes.

While individual microfluidic reactors may never treat sufficient volumes of drinking water to meet human daily needs, the purpose of this work was to demonstrate the importance of inter-electrode spacing on electrocatalytic reactor designs and potential to reduce addition of salt to drinking waters. Moreover, the MEMS fabricated microfluidic reactors offers a robust and highly reproducible platform to study electrocatalytic reactions in a way that allows separation of mass

transport rates (from bulk solution to electrode surfaces) from surface electrode reactions, and potentially even back diffusion of reaction by-products into the bulk solution.

Acknowledgement

This work was partially funded by the National Science Foundation (EEC-1449500) Nanosystems Engineering Research Center for Nanotechnology-Enabled Water Treatment. We would like to thank King Saud University for their fund through Researchers Supporting Project number (RSPD2023R529), King Saud University, Riyadh, Saudi Arabia. We would like to thank the staff of the Center for Solid State Electronics Research (CSSER) at Arizona State University (ASU) Tempe AZ, for their cleanroom and nanofabrication training and technical support. The authors also acknowledge the support of the Centre National de la Recherche Scientifique (CNRS) and the funding received from the European Union's Horizon 2020 research and innovation program under the Marie Sklodowska-Curie grant agreement No 843870.

References

(1) Garcia-segura, S.; Ocon, J. D.; Nan, M. Electrochemical Oxidation Remediation of Real Wastewater Effluents — A Review. *Process Safety and Environmental Protection* **2017**, *113*, 48–67. https://doi.org/10.1016/j.psep.2017.09.014.

(2) Garcia-Segura, S.; Lanzarini-Lopes, M.; Hristovski, K.; Westerhoff, P. Electrocatalytic Reduction of Nitrate: Fundamentals to Full-Scale Water Treatment Applications. *Appl Catal B* **2018**, *236* (May), 546–568. https://doi.org/10.1016/j.apcatb.2018.05.041.

(3) Feng, Y.; Yang, L.; Liu, J.; Logan, B. E. Electrochemical Technologies for Wastewater Treatment and Resource Reclamation. *Environ Sci (Camb)* **2016**, *2* (5), 800–831.

(4) Mousset, E.; Puce, M.; Pons, M. Advanced Electro-Oxidation with Boron-Doped Diamond for Acetaminophen Removal from Real Wastewater in a Microfluidic Reactor : Kinetics and Mass-Transfer Studies. *ChemElectroChem* **2019**, 2908–2916. https://doi.org/10.1002/celc.201900182.

(5) Panizza, M.; Cerisola, G. Direct and Mediated Anodic Oxidation of Organic Pollutants. *Chem Rev* **2009**, *109* (12), 6541–6569.

(6) Martínez-Huitle, C. A.; Rodrigo, M. A.; Sirés, I.; Scialdone, O. Single and Coupled Electrochemical Processes and Reactors for the Abatement of Organic Water Pollutants: A Critical Review. *Chem Rev* **2015**, *115* (24), 13362–13407.

(7) Pérez, J. F.; Llanos, J.; Sáez, C.; López, C.; Cañizares, P.; Rodrigo, M. A. A Micro Fluidic Fl Ow-through Electrochemical Reactor for Wastewater Treatment : A Proof-of-Concept. *Electrochem commun* **2017**, *82* (July), 85–88. https://doi.org/10.1016/j.elecom.2017.07.026.

(8) Flores, K.; Cerrón-Calle, G. A.; Valdes, C.; Atrashkevich, A.; Castillo, A.; Morales, H.; Parsons, J. G.; Garcia-Segura, S.; Gardea-Torresdey, J. L. Outlining Key Perspectives for the Advancement of Electrocatalytic Remediation of Nitrate from Polluted Waters. *ACS ES and T Engineering*. American Chemical Society May 13, 2022, pp 746–768. https://doi.org/10.1021/acsestengg.2c00052.

(9) Cerrón-Calle, G. A.; Senftle, T. P.; Garcia-Segura, S. Strategic Tailored Design of Electrocatalysts for Environmental Remediation Based on Density Functional Theory (DFT) and Microkinetic Modeling. *Current Opinion in Electrochemistry*. Elsevier B.V. October 1, 2022. https://doi.org/10.1016/j.coelec.2022.101062.

(10) van Langevelde, P. H.; Katsounaros, I.; Koper, M. T. M. *Electrocatalytic Nitrate Reduction for Sustainable Ammonia Production*.

(11) Cerrón-Calle, G. A.; Fajardo, A. S.; Sánchez-Sánchez, C. M.; Garcia-Segura, S. Highly Reactive Cu-Pt Bimetallic 3D-Electrocatalyst for Selective Nitrate Reduction to Ammonia. *Appl Catal B* **2022**, *302*, 120844. https://doi.org/10.1016/j.apcatb.2021.120844.

(12) Mart, C. A.; Rodrigo, M. A.; Sire, I.; Scialdone, O. Single and Coupled Electrochemical Processes and Reactors for the Abatement of Organic Water Pollutants : A Critical Review. *Chemical Review* **2015**. https://doi.org/10.1021/acs.chemrev.5b00361.

(13) Kapałka, A.; Fóti, G.; Comninellis, C. Basic Principles of the Electrochemical Mineralization of Organic Pollutants for Wastewater Treatment. In *Electrochemistry for the Environment*; Springer, 2010; pp 1–23.

(14) Walker, W. S.; Bezerra Cavalcanti, E.; Atrashkevich, A.; Fajardo, A. S.; Brillas, E.; Garcia-Segura, S. Mass Transfer and Residence Time Distribution in an Electrochemical Cell with an Air-Diffusion Electrode: Effect of Air Pressure and Mesh Promoters. *Electrochim Acta* **2021**, *378*, 138131. https://doi.org/10.1016/j.electacta.2021.138131.

(15) Coñizares, P.; García-Gómez, J.; Fernández de Marcos, I.; Rodrigo, M. A.; Lobato, J. Measurement of Mass-Transfer Coefficients by an Electrochemical Technique. *J Chem Educ* **2006**, *83* (8), 1204–1207. https://doi.org/10.1021/ed083p1204.
(16) Srisurichan, S.; Jiraratananon, R.; Fane, A. G. Mass Transfer Mechanisms and Transport Resistances in Direct Contact Membrane Distillation Process. *J Memb Sci* **2006**, *277* (1–2), 186–194.
(17) Vakhrushev, A.; Molchanov, E. Simulation of Nanocomposite Coating Created by Electrocodeposition Method. **2016**, No. May.
(18) Garcia-Segura, S.; Nienhauser, A. B.; Fajardo, A. S.; Bansal, R.; Coonrod, C. L.; Fortner, J. D.; Marcos-Hernández, M.; Rogers, T.; Villagran, D.; Wong, M. S. Disparities between Experimental and Environmental Conditions: Research Steps toward Making Electrochemical Water Treatment a Reality. *Curr Opin Electrochem* **2020**, *22*, 9–16.
(19) Herrmann, J.-M. Heterogeneous Photocatalysis: Fundamentals and Applications to the Removal of Various Types of Aqueous Pollutants. *Catal Today* **1999**, *53* (1), 115–129.
(20) Wang, N.; Zhang, X.; Chen, B.; Song, W.; Chan, N. Y.; Chan, H. L. W. Microfluidic Photoelectrocatalytic Reactors for Water Purification with an Integrated Visible-Light Source. *Lab Chip* **2012**, *12* (20), 3983–3990.
(21) Wang, N.; Zhang, X.; Wang, Y.; Yu, W.; Chan, H. L. W. Microfluidic Reactors for Photocatalytic Water Purification. *Lab Chip* **2014**, *14* (6), 1074–1082. https://doi.org/10.1039/c3lc51233a.
(22) Mousset, E.; Puce, M.; Pons, M. Advanced Electro□Oxidation with Boron□Doped Diamond for Acetaminophen Removal from Real Wastewater in a Microfluidic Reactor: Kinetics and Mass□Transfer Studies. *ChemElectroChem* **2019**, *6* (11), 2908–2916.
(23) Shahbabaei, M.; Kim, D. Advances in Nanofluidics for Water Purification and Filtration: Molecular Dynamics (MD) Perspective. *Environ Sci Nano* **2021**.
(24) Kuleshova, J.; Hill-Cousins, J. T.; Birkin, P. R.; Brown, R. C. D.; Pletcher, D.; Underwood, T. J. The Methoxylation of N-Formylpyrrolidine in a Microfluidic Electrolysis Cell for Routine Synthesis. *Electrochim Acta* **2012**, *69*, 197–202. https://doi.org/10.1016/j.electacta.2012.02.093.
(25) Kuleshova, J.; Hill-Cousins, J. T.; Birkin, P. R.; Brown, R. C. D.; Pletcher, D.; Underwood, T. J. A Simple and Inexpensive Microfluidic Electrolysis Cell. *Electrochim Acta* **2011**, *56* (11), 4322–4326. https://doi.org/10.1016/j.electacta.2011.01.036.
(26) Amemiya, F.; Horii, D.; Fuchigami, T.; Atobe, M. Self-Supported Paired Electrosynthesis Using a Microflow Reactor Without Intentionally Added Electrolyte. *J Electrochem Soc* **2008**, *155* (11), E162. https://doi.org/10.1149/1.2975823.
(27) Ziogas, A.; Kolb, G.; O'Connell, M.; Attour, A.; Lapicque, F.; Matlosz, M.; Rode, S. Electrochemical Microstructured Reactors: Design and Application in Organic Synthesis. *J Appl Electrochem* **2009**, *39* (12), 2297–2313. https://doi.org/10.1007/s10800-009-9939-6.
(28) He, P.; Watts, P.; Marken, F.; Haswell, S. J. Electrolyte Free Electro-Organic Synthesis: The Cathodic Dimerisation of 4-Nitrobenzylbromide in a Micro-Gap Flow Cell. *Electrochem commun* **2005**, *7* (9), 918–924. https://doi.org/10.1016/j.elecom.2005.06.013.
(29) Scialdone, O.; Guarisco, C.; Galia, A. Oxidation of Organics in Water in Microfluidic Electrochemical Reactors: Theoretical Model and Experiments. *Electrochim Acta* **2011**, *58* (1), 463–473. https://doi.org/10.1016/j.electacta.2011.09.073.

(30) Scialdone, O.; Galia, A.; Sabatino, S.; Vaiana, G. M.; Agro, D.; Busacca, A.; Amatore, C. Electrochemical Conversion of Dichloroacetic Acid to Chloroacetic Acid in Conventional Cell and in Two Microfluidic Reactors. *ChemElectroChem* **2014**, *1* (1), 116–124. https://doi.org/10.1002/celc.201300216.
(31) Cao, M.; Wu, D.; Cao, R. Recent Advances in the Stabilization of Platinum Electrocatalysts for Fuel□Cell Reactions. *ChemCatChem* **2014**, *6* (1), 26–45.
(32) Kettler, P. B. Platinum Group Metals in Catalysis: Fabrication of Catalysts and Catalyst Precursors. *Org Process Res Dev* **2003**, *7* (3), 342–354.
(33) Fajardo, A. S.; Westerhoff, P.; Sanchez-Sanchez, C. M.; Garcia-Segura, S. Earth-Abundant Elements a Sustainable Solution for Electrocatalytic Reduction of Nitrate. *Appl Catal B* **2021**, *281* (June 2020), 119465. https://doi.org/10.1016/j.apcatb.2020.119465.
(34) Bard, A. J.; Faulkner, L. R. *Fundamentals and Applications*; Wiley New York, 2001; Vol. 2.
(35) Bolton, J. R.; Bircher, K. G.; Tumas, W.; Tolman, C. A. Figures-of-Merit for the Technical Development and Application of Advanced Oxidation Technologies for Both Electric- and Solar-Driven Systems. *Pure and Applied Chemistry* **2001**, *73* (4), 627–637. https://doi.org/10.1351/pac200173040627.
(36) Lanzarini-Lopes, M.; Garcia-Segura, S.; Hristovski, K.; Westerhoff, P. Electrical Energy per Order and Current Efficiency for Electrochemical Oxidation of P-Chlorobenzoic Acid with Boron-Doped Diamond Anode. *Chemosphere* **2017**, *188*, 304–311. https://doi.org/10.1016/j.chemosphere.2017.08.145.
(37) Everett, D. H. Manual of Symbols and Terminology for Physicochemical Quantities and Units, Appendix II: Definitions, Terminology and Symbols in Colloid and Surface Chemistry. *Pure Appl. Chem* **1972**, *31* (4), 577–638.
(38) Trellu, C.; Chaplin, B. P.; Coetsier, C.; Esmilaire, R.; Cerneaux, S.; Causserand, C.; Cretin, M. Electro-Oxidation of Organic Pollutants by Reactive Electrochemical Membranes. *Chemosphere* **2018**, *208*, 159–175. https://doi.org/10.1016/j.chemosphere.2018.05.026.
(39) Tchobanoglous, G.; Burton, F. L.; Stensel, H. D. Wastewater Engineering. *Management* **1991**, *7* (1), 4.
(40) Arun Prasad, M.; Sangaranarayanan, M. V. Analysis of the Diffusion Layer Thickness, Equivalent Circuit and Conductance Behaviour for Reversible Electron Transfer Processes in Linear Sweep Voltammetry. *Electrochim Acta* **2004**, *49* (3), 445–453. https://doi.org/10.1016/j.electacta.2003.05.003.
(41) Reuben, C.; Galun, E.; Cohen, H.; Tenne, R.; Kalish, R.; Muraki, Y.; Hashimoto, K.; Fujishima, A.; Butler, J. M.; Lévy-Clément, C. Efficient Reduction of Nitrite and Nitrate to Ammonia Using Thin-Film B-Doped Diamond Electrodes. *Journal of Electroanalytical Chemistry* **1995**, *396* (1–2), 233–239.
(42) Kuang, P.; Natsui, K.; Einaga, Y. Comparison of Performance between Boron-Doped Diamond and Copper Electrodes for Selective Nitrogen Gas Formation by the Electrochemical Reduction of Nitrate. *Chemosphere* **2018**, *210*, 524–530.
(43) Atrashkevich, A.; Fajardo, A. S.; Westerhoff, P.; Walker, W. S.; Sánchez-Sánchez, C. M.; Garcia-Segura, S. Overcoming Barriers for Nitrate Electrochemical Reduction: By-Passing Water Hardness. *Water Res* **2022**, *225*, 119118. https://doi.org/10.1016/j.watres.2022.119118.

(44) dos Santos, E. V.; Sena, S. F. M.; da Silva, D. R.; Ferro, S.; De Battisti, A.; Martínez-Huitle, C. A. Scale-up of Electrochemical Oxidation System for Treatment of Produced Water Generated by Brazilian Petrochemical Industry. *Environmental Science and Pollution Research* **2014**, *21* (14), 8466–8475. https://doi.org/10.1007/s11356-014-2779-x.

Supporting Information: MICROFLUIDIC FLOW-THROUGH REACTORS MINIMIZE ENERGY REQUIREMENTS OF ELECTROCHEMICAL WATER TREATMENT WITHOUT ADDING SUPPORTING ELECROLYTES

Authors: Omar Alrehaili, Ana S. Fajardo, Sergi Garcia-Segura, Paul Westerhoff

Electrodes Preparation

All electrodes used in this work were made of platinum (Pt) and prepared in the lab. Silicon (Si) wafers with the two sizes were cleaned and prepared as substrates for all devices. Due to its high corrosion resistance and ability to not getting poisoned by reduction by-products, platinum electrodes prove to be excellent electrocatalysts for nitrate/nitrite reduction[1–3]. Thermal evaporation technique was used to coat platinum on wafers with a Lesker #3 Thermal Evaporator. At first, 100 nm thickness layer of platinum was coated directly to Si wafers. However, the high stress film of platinum caused a detachment of the coated layer from the wafer after cleaning with just water. Therefore, an adhesive layer (10 nm) of titanium that has a relatively lower stress film was coated first on the wafer followed by 100 nm layer of platinum to achieve stability of the metal on the wafers. Preparing electrodes by thermal evaporation technique results in a homogeneous and smooth electrodes surface to avoid friction forces that might increase in microchannel as reported in other work[4].

1. Microfluidic Device Fabrication

Microfluidic devices were fabricated based on microelectromechanical system (MEMS) techniques where the interelectrode distance (the distance between electrodes) is less than 50 μm (~40 μm). The fabrication involves soft lithography for etching channels on epoxy polymer (SU-

8), and building a delivery system using Polydimethylsiloxane (PDMS). Water flows in a microchannel between electrodes as a continuous flow system using a syringe pump. The microfluidic device fabrication processes were implemented in a clean room.

Each device has two electrodes, top layer wafer (25 × 10 mm) and bottom layer wafer (60 × 35 mm) coated with Pt as described previously (Figure S1a). Bottom piece wafers (60 × 5 mm) with coated platinum layer were further coated with polymer epoxy (SU-8) by a spin coater as a separation layer between the two electrodes in the device. SU-8 is a common negative photoresist that is used for MEMS fabrication. The thickness of the epoxy layer determines the distance between the two electrodes in the device and it is controlled by the viscosity of the polymer and the spin coat speed. In my microdevices, SU-8 2025 (MicroChem Inc.) was spin coated (2,000 rpm for 30 second) on Pt coated wafer (bottom) followed by a soft baking step (95 □ for 6 min) resulting a thickness layer of ~40 μm.

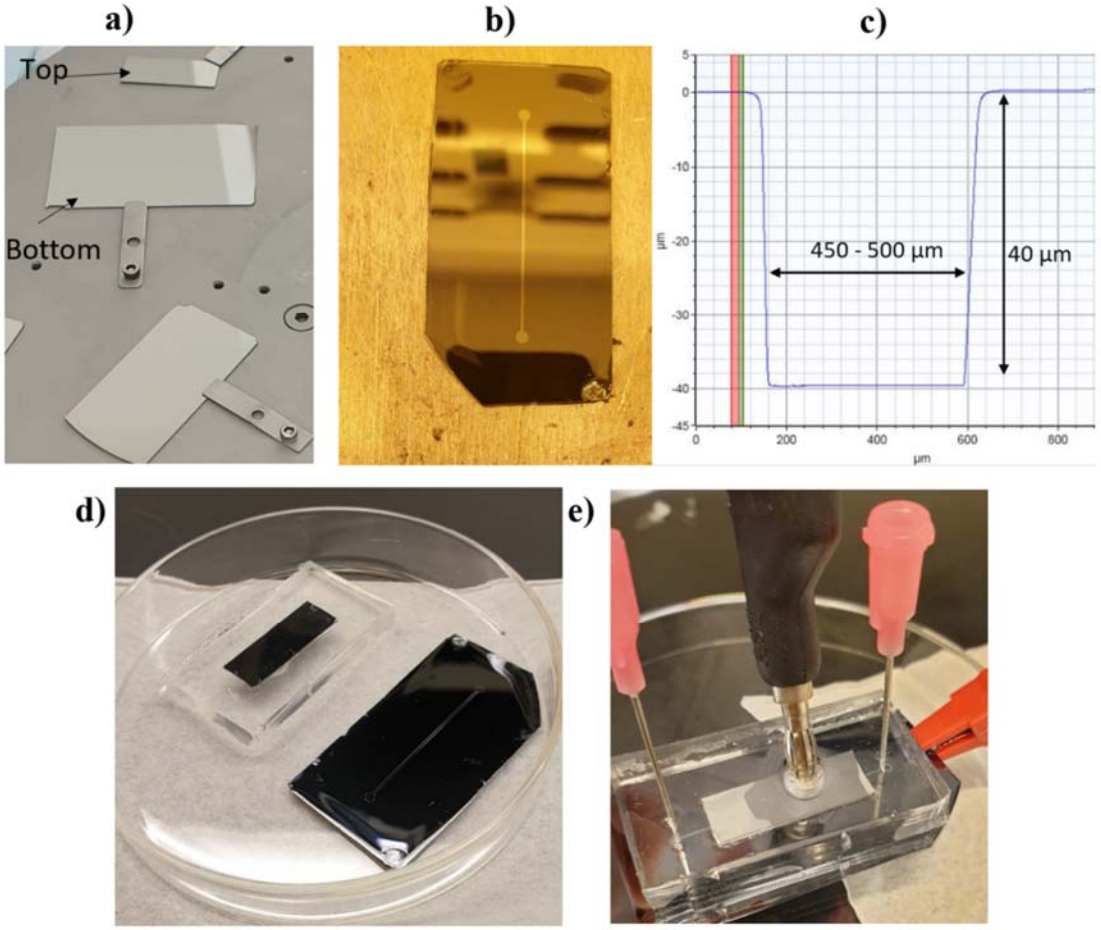

Figure S1: Microfluidic device fabrication steps. a) Two size wafers coated with platinum, top piece (25 × 10 mm) and bottom piece (60 × 35 mm). b) A 500µm channel etched on SU-8 photoresist by a photolithography process. c) A cross section of the fabricated channel with dimensions measured by Bruker XT Profilometer. d) The two parts of the microfluidic device. e) The final look of the microfluidic device connected by two cables at the top substrate (anode) and bottom substrate (cathode).

A channel was etched on the epoxy layer all the way to Pt surface on the wafer. A photo mask therefore was designed where a chromium channel (500 µm wide, 3500 µm long) between to circle reservoirs (2000 µm in diameter) was printed a quartz glass. When UV light is exposed to the negative photoresist (dose = 260 mJ/cm^2) through the mask using an EVG 620 Automated Mask Alignment, the exposed part became solid, unexposed part (reflected by the chromium channel) will be soluble later in the developing process. The substrates were then transferred to

another baking step at 95□ for 6 min. An image of the mask should be visible in the SU-8 photoresist coating. Substrates were then dipped in a developer (SU-8 developer) for 6 minutes to remove the soluble photoresist, followed by a hard baking step (cure) at 180□ for 10 min. The resulted substrate has a visible channel with measured thickness of 40 μm (Figure S1b-c).

In order to connect the microchannel to macro reservoirs, a microfluidic delivery device fabrication (stamp) is needed. The delivery device was made of polydimethylsiloxane (PDMS). Briefly, PDMS (Sylgard 184 Silicone Elastomer kit, Dow Corning) was mixed with its curing agent (Dow Corning Sylgard 184 Silicone Elastomer Curing Agent) at a volumetric ratio of 10:1 under a vacuum. PDMS solution was cured for 2 h at 65□ before it was cast onto the top piece of silicon wafer coated with Pt and hardened for 48 hours at room temperature ~22°C. PDMS was peeled from the mold and ready for hole interconnecting. Needles, 20 gauge, were purchased from Kontes (868280-2001) and sharpen by Dremel Multipro 395. A compressed seal is formed around the needle and oxygen plasma was used for the top and bottom parts to attach them together (Figure S1d). The process of coring involves; using a sharpened needle to make a hole, and removing it, inserting another unsharpened needle in the hole, and connecting the needle with a luer connector (silicon tubes). Figure S1e shows the final shape of device ready to be connected to a power supply.

2. Specific Charge for Nitrite Conversion

The specific charge, the rate of energy consumption over volume, was calculated for nitrite conversion in both reactors. The microfluidic reactor showed lower specific charge needs as it requires lower energy due to the relatively faster nitrite abatement rate. Figure S2 showed specific charge over nitrite conversion for the batch and microfluidic reactors.

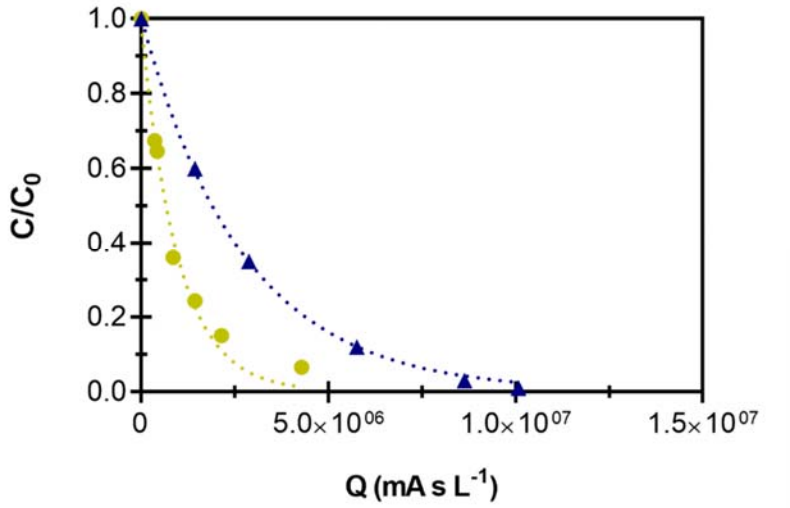

Figure S2. Specific charge (Q) over nitrite conversion for batch reactor (▲) and microfluidic reactor ( ). Current density is fixed at j = 18 mA/cm^2. Initial concentration of nitrite is = 50 mg-N/L and conductivity was 0.53 mS/cm^2.

References

(1) Cao, M.; Wu, D.; Cao, R. *ChemCatChem* **2014**, *6* (1), 26–45.

(2) Kettler, P. B. *Org. Process Res. Dev.* **2003**, *7* (3), 342–354.

(3) Garcia-Segura, S.; Lanzarini-Lopes, M.; Hristovski, K.; Westerhoff, P. *Appl. Catal. B Environ.* **2018**, *236* (May), 546–568.

(4) Pérez, J. F.; Llanos, J.; Sáez, C.; López, C.; Cañizares, P.; Rodrigo, M. A. *Electrochem. commun.* **2017**, *82* (July), 85–88.